Advanced Physics Lab I

Lab Report #3

Group 1
Noah Horne, Luka Burduli

23.09.2024

Dr. Veit Wagner
Tim Jesko Söcker

We hereby declare that we (Luka Burduli and Noah Horne) are the sole authors of this lab report and have not used any sources other than those listed in the bibliography and identified as references throughout the report.

_____ _____

Contents

1 Abstract

2 Introduction & Theory

This experiment aims to understand the underlying properties of light, particularly its polarization. Through a classical perspective, light can be classified as an electromagnetic wave and therefore described by a simplification of Maxwell's Equations,

$$\nabla^2 \vec{A} - \frac{1}{v^2}\frac{\partial^2 \vec{A}}{\partial t^2} = 0 \tag{1}$$

where v is the velocity of light and $\vec{A}$ is either an electric field strength, denoted by $\vec{E}$, or the density of a magnetic flux field, $\vec{B}$. If one assumes that the material does not absorb the light (through some process such as heating or ionization), then the solution of equation 1 can be expressed as the superposition of waves which have a constant wave vector $\vec{k}$, meaning they point in one direction, and have a constant frequency, ω. Waves of this family are also known as monochromatic plane waves, due to their aforementioned behavior. The solution to the equation above can expressed as an arbitrary superposition of these waves:

$$\vec{A} = \vec{A}_0 e^{i(\omega t - \vec{k}\cdot\vec{r})} = \vec{A}_0(\cos(\omega t - \vec{k}\cdot\vec{r}) + i\sin(\omega t - \vec{k}\cdot\vec{r})) \tag{2}$$

Where $\vec{A}$ is again the electric field strength or magnetic flux density, ω is the angular frequency, $\vec{k}$ is a constant wave vector, i is the imaginary number $i = \sqrt{-1}$ and $\vec{r}$ which is an arbitrary position vector in space. Furthermore, the magnitude of the wave vector $\vec{k}$ is directly dependent on the refractive index n of the media through and the angular frequency ω of the wave.

$$|\vec{k}| = k = \frac{2\pi}{\lambda}n = \frac{\omega}{c}n \tag{3}$$

Due to the constant nature of the wave vector in monochromatic plane waves, this implicitly implies that the refractive index n of a medium is inversely proportional to the angular frequency ω at which the wave propagates. Rearranging formula 3, it is clear:

$$k = \frac{\omega}{c}n \implies \omega = \frac{kc}{n} \implies \omega \propto \frac{1}{n} \tag{4}$$

Using this knowledge, one can better understand the nature of a reflected-refracted wave at the boundary of two media of different refractive index n. When a wave hits the boundary of two media with refractive indices n_1 and n_2, it is clear from equation 4 that one will observe a shift in the velocity of the wave, as:

$$c = \lambda\frac{\omega}{2\pi} \tag{5}$$

At the boundary between two media, the incident wave, the reflected wave, and the

transmitted wave are all co-planar to a plane called the 'plane of incidence'. At the interface of a media, it is clear that the projection of the incident wave $\vec{A}_i$ and the reflected wave $\vec{A}_r$ onto the boundary surface have to be equal at both sides of the interface. To algebraically formulate this, one writes:

$$\vec{A}_{\tau,i}e^{i(\omega_i t-\vec{k}_i\cdot\vec{r})}+\vec{A}_{\tau,r}e^{i(\omega_r t-\vec{k}_r\cdot\vec{r})}=\vec{A}_{\tau,t}e^{i(\omega_t t-\vec{k}_t\cdot\vec{r})} \tag{6}$$

Where $\vec{r}$ now lies on the interface plane. In order for these requirements instantiated by this equation to be fulfilled, it is necessary for the exponential components of each term to be equal:

$$\begin{aligned}&\implies \omega_i t-\vec{k}_i\cdot\vec{r}=\omega_r t-\vec{k}_r\cdot\vec{r}=\omega_t t-\vec{k}_t\cdot\vec{r}\\ &\implies \omega_i=\omega_r=\omega_t \quad\wedge\quad k_{\tau,i}=k_{\tau,r}=k_{\tau,t}\end{aligned} \tag{7}$$

Since it is known that the k's above are projections of the wave vector onto the incident plane, one can rewrite equation 7 to find the incident and reflecting angle as:

$$k_i=k_r \implies \sin\theta_1=\sin\theta_2 \implies \underline{\theta_1=\theta_2} \tag{8}$$

Similarly, one can apply formula 3 to relate the angles of the incident and transmitted waves with respect to the refractive indices of the mediums through which they propagate by equating $k_{\tau,i}$ and $k_{\tau,t}$.

$$k_{\tau,i}=k_{\tau,t} \implies \frac{2\pi}{\lambda}n_1\sin\theta_1=\frac{2\pi}{\lambda}n_2\sin\theta_2 \implies \underline{n_1\sin\theta_1=n_2\sin\theta_2} \tag{9}$$

The equation derived above is Snell's law, and is valid for any form of the wave entering an interface system–including different polarization types. To elaborate, polarization can occur at the boundary between two media in two main ways, via either transverse electric (TE) polarization, or transverse magnetic (TM) polarization. When considering TE polarization, the electric field can be observed orthogonal to the plane of incidence—this form of polarization (TE) is also called s- polarization. Alternatively, when considering TM polarization, it is the magnetic flux density component of the EM wave which appears normal to the plane of incidence—this form of polarization (TM) is alternatively denoted as p- polarization. The only important distinction made between these polarizations is the orthogonality of the electric field in relation to the plane of incidence, s- polarization when $\vec{E}$ is orthogonal, and p- polarization when $\vec{E}$ is parallel or co-planar. In both cases, the polarization is considered linear, as the direction of oscillation of the electric field is invariant under polarization.

Using these properties of the two polarization types, one can establish clear boundary conditions for the coplanar electric field $\vec{E}^{\parallel}$ case at the boundary, and the orthogonal electric field $\vec{E}^{\perp}$ case at the boundary. Immediately following from equation 6, the conditions for the electric and magnetic field for s-polarization and p-polarization respectively are:

$$\underbrace{E_i^{\perp} + E_r^{\perp} = E_t^{\perp}}_{\text{s-polarization}} \implies \underbrace{B_i^{\perp} + B_r^{\perp} = B_t^{\perp}}_{\text{p-polarization}} \tag{10}$$

$$\underbrace{-B_i^{\parallel}\cos\theta_1 + B_r^{\parallel}\cos\theta_1 = -B_t^{\parallel}\cos\theta_2}_{\text{s-polarization}} \implies \underbrace{-E_i^{\parallel}\cos\theta_1 + E_r^{\parallel}\cos\theta_1 = -E_t^{\parallel}\cos\theta_2}_{\text{p-polarization}} \tag{11}$$

By applying the orthogonality of the electric and magnetic fields, one can rearrange these equations to yield:

$$\underbrace{E_i^{\perp} + E_r^{\perp} = E_t^{\perp}}_{\text{s-polarization}} \implies \underbrace{n_1E_i^{\parallel} + n_1E_r^{\parallel} = n_2E_t^{\parallel}}_{\text{p-polarization}} \tag{12}$$

$$\underbrace{-n_1E_i^{\perp}\cos\theta_1 + n_1E_r^{\perp}\cos\theta_1 = -n_2E_t^{\perp}\cos\theta_2}_{\text{s-polarization}} \implies \underbrace{-E_i^{\parallel}\cos\theta_1 + E_r^{\parallel}\cos\theta_1 = -E_t^{\parallel}\cos\theta_2}_{\text{p-polarization}} \tag{13}$$

Using 12 and 13, Fresnel's coefficients for reflection and transmission can be derived for s-polarization and p-polarization respectively:

$$r^{\perp} = \frac{E_r^{\perp}}{E_i^{\perp}} = \frac{n_1\cos\theta_1 - n_2\cos\theta_2}{n_1\cos\theta_1 + n_2\cos\theta_2} \tag{14}$$

$$t^{\perp} = \frac{E_t^{\perp}}{E_i^{\perp}} = \frac{2n_1\cos\theta_1}{n_1\cos\theta_1 + n_2\cos\theta_2} \tag{15}$$

$$r^{\parallel} = \frac{E_r^{\parallel}}{E_i^{\parallel}} = \frac{n_2\cos\theta_1 - n_1\cos\theta_2}{n_2\cos\theta_1 + n_1\cos\theta_2} \tag{16}$$

$$t^{\parallel} = \frac{E_t^{\perp}}{E_i^{\perp}} = \frac{2n_1\cos\theta_1}{n_2\cos\theta_1 + n_1\cos\theta_2} \tag{17}$$

In the context of this experiment, the Fresnel coefficients serve as a quantifier of the behavior of light as it interacts with an interface between two media. Throughout the entirety of this investigation, the two media responsible for this interface are glass and air, each with their own respective refractive indices. For air, its refractive index $n_{air} \approx 1$. For glass, its refractive index $n_{glass} > n_{air}$, and is approximately $n_{glass} \approx 1.63$ (Wagner & Söcker, 2024). Substituting these values into Snell's law (equation 9), one achieves a more relevant form of the equation for the context of this experiment, where α is the incident angle and β is the refracted angle:

$$\sin(\alpha) = n_{glass}\sin(\beta) \tag{18}$$

Leading to expressions of Fresnel's reflection coefficients as seen below.

$$r^{\perp} = \frac{\cos\alpha - n_{glass}\cos\beta}{\cos\alpha + n_{glass}\cos\beta} \tag{19}$$

$$r^{\parallel} = \frac{n_{glass}\cos\alpha - \cos\beta}{n_{glass}\cos\alpha + \cos\beta} \tag{20}$$

By using this more applied formula in the context of Fresnel's coefficients, one can eliminate terms containing n_{glass} and β through some basic trigonometry. Doing so yields an expression for the Fresnel reflection coefficients expressed solely in terms of the incident angle, α and the refractive index of glass n_{glass} as seen below.

$$r^{\perp} = -\frac{\left(\sqrt{n_{glass}^2 - \sin^2\alpha} - \sqrt{1 - \sin^2\alpha}\right)^2}{n_{glass}^2 - 1} \tag{21}$$

$$r^{\parallel} = \frac{n_{glass}^2\sqrt{1 - \sin^2\alpha} - \sqrt{n_{glass}^2 - \sin^2\alpha}}{n_{glass}^2\sqrt{1 - \sin^2\alpha} + \sqrt{n_{glass}^2 - \sin^2\alpha}} \tag{22}$$

These expressions of the Fresnel coefficients will be of vital importance in verifying the accuracy of the data collected during the analysis and empirical calculation of said coefficients, as it expresses the coefficient in terms of only one variable parameter, the incident angle α. As much of the measurements taken during the experiment will be based off of the intensity after polarization, an alternative expression for the reflection coefficient is necessary to ease the calculation of the Fresnel coefficients based off of empirical measurements. To do so, the notion of the reflectance R of a media is introduced, which is defined as the ratio of the incident and reflected intensities $I_{i,r}$ of a wave interacting at the interface of the medium.

$$R^{\perp,\parallel} = \frac{I_r^{\perp,\parallel}}{I_i^{\perp,\parallel}} \overbrace{\Longrightarrow}^{I\propto E^2} R^{\perp,\parallel} = \frac{|E_r^{\perp,\parallel}|^2}{|E_i^{\perp,\parallel}|^2} = |r^{\perp,\parallel}|^2 \tag{23}$$

Rearranging equation 23, one arrives at the relationship which will be used to calculate the Fresnel reflection coefficients from the intensity data collected during the investigation.

$$|r^{\perp,\parallel}| = \sqrt{\frac{I_r^{\perp,\parallel}}{I_i^{\perp,\parallel}}} \tag{24}$$

In Physics, it is often times significant and valuable to analyze the properties of the parameters responsible for a calculated value such that the calculated value is maximized or minimized. This process strengthens ones understanding of the property, and can give rise to new phenomena. In the case of the Fresnel reflection coefficient for p-polarization, a minimum value (0) occurs when $\alpha + \beta = \frac{\pi}{2}$. Alternatively, when the angle between the reflected and refracted rays form an angle of $\pi/2$ radians. The incident angle α_B at which this phenomena occurs is called the Brewster Angle (Wagner & Söcker, 2024). Substituting the Brewster angle into Snell's law, one can calculate the refractive index of glass and vice versa should it be known.

$$\tan\alpha_B = n_{glass} \tag{25}$$

Now let us consider an alternative case where light is linearly polarized via a polarizer,

rather than by reflection off of an alternate medium. When light is polarized in this manner, its polarization vector lies along the polarization axis, which is given by the rotation of the polarizer through which it passes. After passing through the polarizer, the light only oscillates along the polarization axis. Should this polarized light then pass through another polarizer–which is often denoted as the analyzer–then the electric field component of the light coming out through the analyzer will have an intensity directly related to the angle at which the analyzers polarization axis lies in relation to the polarization axis of the already polarized light. This relationship is given by,

$$E_A = E_0 \cos\phi \tag{26}$$

where ϕ is the angle between the analyzers polarization axis and the lights polarization axis. Extrapolating this result by applying the proportionality between the square of the electric field and the intensity ($I \propto E^2$), one can rewrite the formula in terms of the lights intensity:

$$I_A = I_0 \cos^2\phi \qquad \text{(Malus' Law)} \tag{27}$$

The law above applies to linear polarizers, and is called Malus' Law. However, there are also other types of polarization besides linear polarization. Specifically, circular polarization occurs when a linearly polarized light beam passes through a medium which has two different refractive indices. Materials of this type are called anisotropic, more specifically, birefringent crystals. The refractive indices of a birefringent crystal are called the ordinary refractive index n_{OR}, and the extraordinary refractive index n_{EO}. These differing refractive indices give rise to two different velocities of sound travelling through the material.

$$n_{OR} = \frac{c}{v_{OR}} \tag{28}$$

$$n_{EO} = \frac{c}{v_{EO}} \tag{29}$$

Due to the differing speeds of these wave caused by the birefringent crystal causes the wave to split into two waves. As the waves propagate through the birefringent crystals, a phase difference is accumulated. A plate of birefringent crystal that yields a phase difference of $\pi/2$ is called a quarterwave plate. For the purposes of this investigation, the effect of a quarterwave plate on linearly polarized light will be examined. It is clear by the theory given that linearly polarized light incident on a quarterwave plate will split into two different waves, and become what is regarded as ellipticaly polarized. elliptic polarization is caused by the superposition of the two orthogonal waves of differing magnitudes, leading to the wave travelling in an elliptical manner. In the case where the angle between the linearly polarized light and the ordinary and extraordinary axes is ± 45 degrees, the transmitted linearly polarized wave emerges circularly polarized, with equal components along the ordinary and extraordinary axis of the birefringent

crystal. This investigation applies this theory to only linearly polarized light, and analyzes the intensity of circularly polarized light after it again passes through a linear polarizer.

When two different quarterwave plates are placed one after the other, the waves undergo a phase shift of π relative to eachother. Linearly polarized light entering a halfwave plate emerges likewise linearly polarized if aligned at 45 degrees from one another. In the investigation, the behavior of polarized light passing through a halfwave plate is analyzed for different angles of the polarizer and analyzer positioned on opposite sides of the halfwave plate.

3 Experimental Procedure

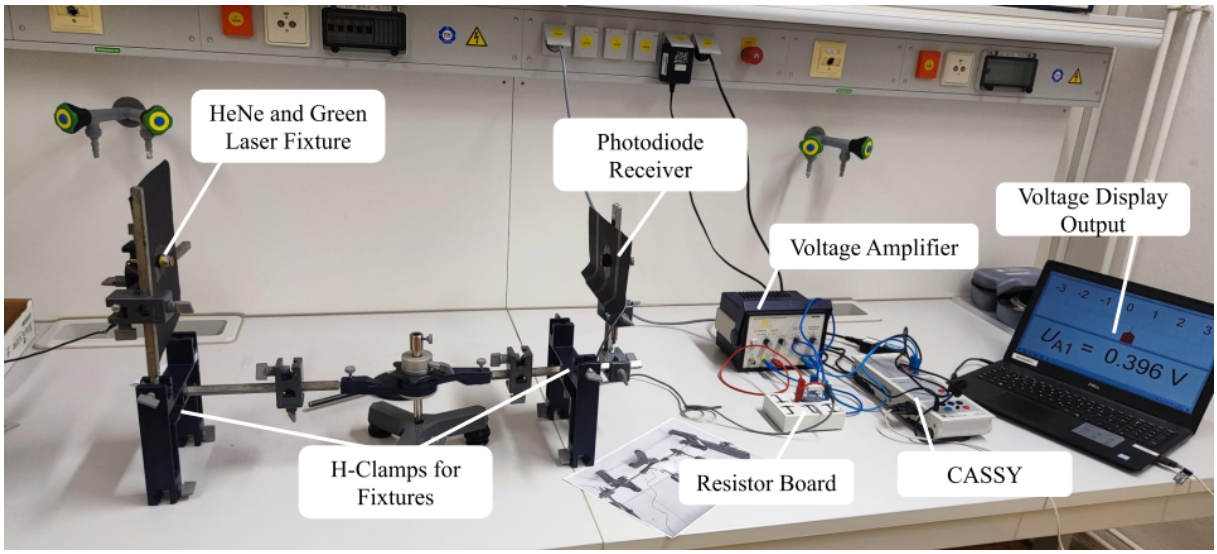

Figure 1: Measuring Stability of Laser Setup

To determine the best fit laser for the remainder of the investigation, the first setup focuses on the analysis of stability for two types of lasers (HeNe and Green) to qualitatively assess their behavior over time. To do so, a photodiode receiver equipped with a beam-stopper is positioned diametrically opposed to the laser. The photodiodes' signal is then passed through a resistor to create a measureable potential difference. This voltage is then amplified via a voltage amplifier before passed to a digital sensor readout on the CASSY, displayed on a computer. After measuring each of the lasers signals for approximately 15 minutes, the plots of two signals' intensities with respect to time were analyzed, and the more stable laser was picked for the remainder of the investigation. The signal of the photodiode was also noted with no laser incident on it in a dark room, to pick up any background radiation from scattered photons or due to the chaotic thermal movement of electrons along the semiconductors present in the photodiode. For this setup, no formulas were necessary as the analysis was purely qualitative–such as looking for bumps and fluctuations in the graph.

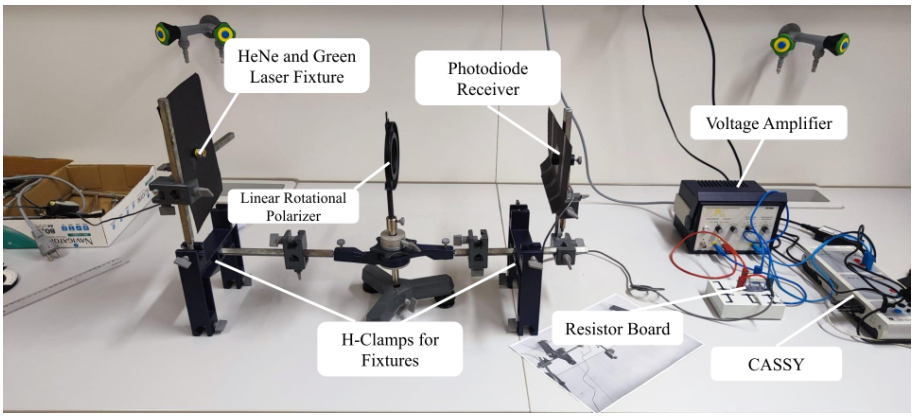

Figure 2: Malus' Law Measurement Setup

After the best laser is determined from the first setup, a linear rotating polarizer is placed in between the laser fixture and the photodiode reciever, which acts as an analyzer to the already polarized light of the incident green laser. The intensity was measured in the same way as the first setup, using the voltage across the resistor produced by the signal from the photodiode. In order to determine the angle of polarization of the laser, the analyzer is rotated through between -90 and 90 degrees in steps of 10 degrees. This data is then normalized with respect to the maximum intensity, such that the angle of polarization of the laser can be found by taking the angle of the maximum of the intensity graph. Then, as a means of confirming Malus' Law (equation 27), a plot of the intensities against the cosine of the angle squared is plotted to produce a straight line. The slope is then compared to the theoretical value found by taking the maximum intensity and intensity and angle at 0.

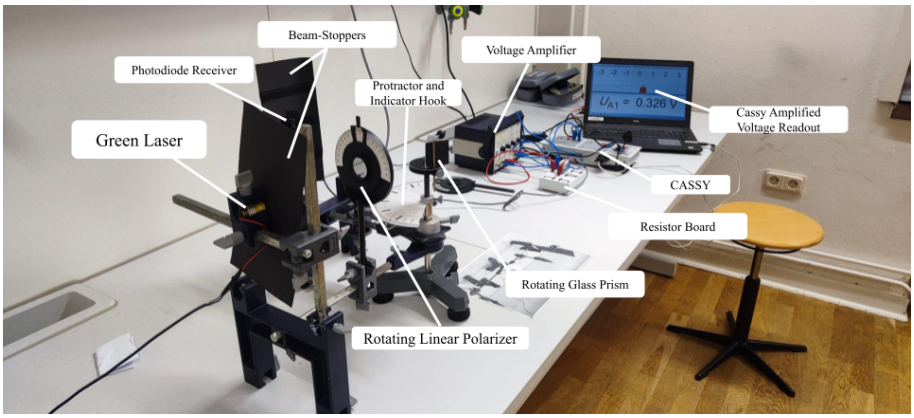

Figure 3: Measuring p-Polarization and s-Polarization Setup

For the third part of the investigation, Fresnel's Reflection coefficients for s- and p-polarization were determined through the analysis of reflected polarized light off of a glass prism. As seen in the figure above, the light from the laser is first passed through a polarizer before landing incident to the glass prism. To switch easily between p and s polarization, the results of the previous setup are used as a means of rotating the laser such that its polarization angle lies

45 degrees from the vertical. Doing so allows one to switch the polarization type of the light on the prism by simply rotating the analyzer to either 90 degrees or 0 degrees. While the intensity of the laser light will drop after moving through the analyzer, this drop will be the same as the relative angle between the light and the polarizer do not change (consistently 45 degrees). For both polarization types, the prism was rotated through a range of angles between 15 to 85 degrees in steps of 5 degrees. This allows to calculate the reflection coefficients by applying formula 24, using the original intensity of the laser as the incident intensity. After the experimental values of fresnel's reflection coefficients were calculated for both types of polarization, equations 21 and 22 were applied to find the theoretical values. One then compared the two plots to determine the theoretical accuracy and applicability of the data gathered.

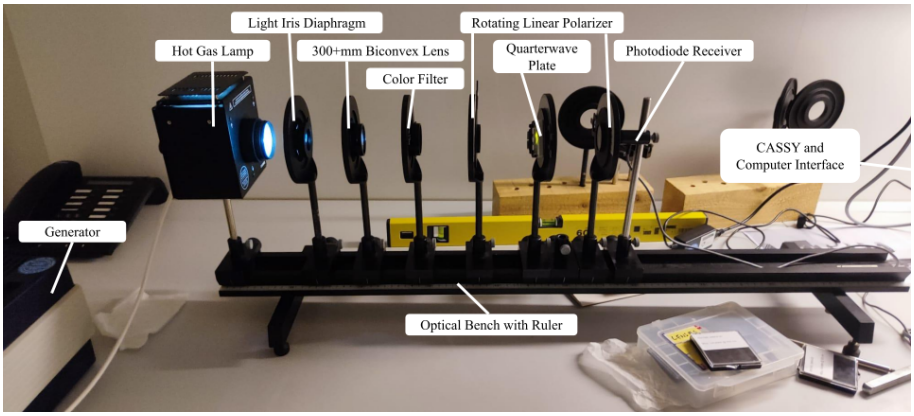

Figure 4: Measuring of intensity from a Quarterwave Plate

For the fourth part of the investigation, the effects of a quarterwave plate on linearly polarized light was examined. More specifically, an optical setup was created which allowed for polarized light to be passed through a birefringent crystal and then analyzed with another polarizer. The resultant signal was then received by a photodiode and results were acquired in the same manner. Before measurements were taken, the minimum and maximum observed intensity from the hot gas lamp were taken to ensure stability–similar to what was done for the HeNe laser and the Green laser. During this process, the lamp is also switched off to allow for the background radiation to be measured as well. With the background radiation and stability of the laser quantified, the behavior of the quarterplate was then examined. To begin, the light from the lamp passes through an Iris Diaphragm to shut off any scattered light. Then it passes through a 300+ mm biconvex lens such that the light is focused on the photodiode reciever, which is placed at roughly 300 mm from the lens. After the biconvex lens, the white light is passed through a color filter. With a more restricted range of wavelengths, more accurate measurements can be taken. After the light is color filtered, it passes through the first polarizer to become linearly polarized. This linearly polarized light then passes through the quarterwave plate, and becomes elliptically polarized. This elliptically polarized light is then sent back through another polarizer, which acts as an analyzer. The photodiode receiver then measures the incident light intensity.

The intensity of the photodiode was measured with respect to the angle of the analyzer for fixed angles of the polarizer of $0°, 30°, 45°, 60°$ and $90°$ respectively. Then, the polarizer will be fixed at $0°$, and the quarterwave plate will be varied by the same angles instead.

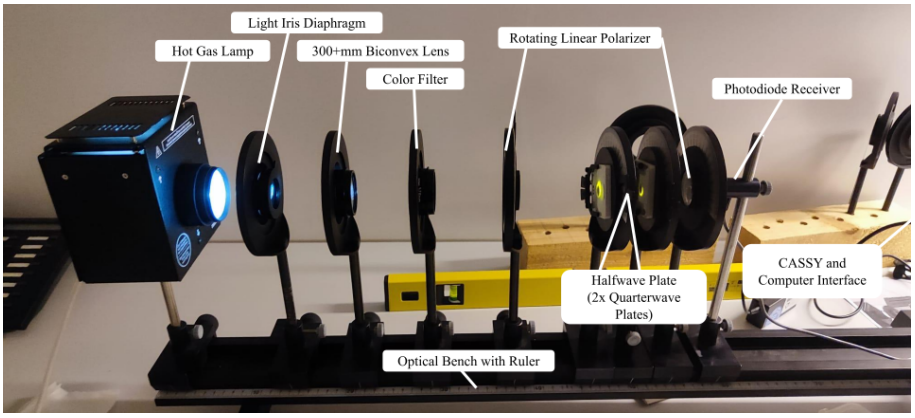

Figure 5: Measuring of intensity from a Halfwave Plate

The last part of this experiment investigates the behavior of a halfwave plate formed by two quarterwave plates. The setup starts by first determining the alignment of the quarterwave plates such that it makes a full half wave plate. To do so, the first linear polarizer was set to 0 degrees, then the linear analyzer at the end was set to 90 degrees. After doing so, the two quarterwave plates were rotated until the transmitted intensity incident on the photodiode was minimized. When the intensity on the photodiode is minimum, this means that the half wave plate does not change the direction of the polarization axis of the linearly polarized light, as when it emerges, it is perpendicular to the 90 degrees, and therefore still in the same direction as when it was initially polarized. After alignment, the intensities dependent on the angle of the analyzer was measured for varying angles of the polarizer $10°, -20°, 30°, -40°$. After these measurements, one of the quarterwave plates was rotated by 90 degrees in its holder, and the resultant polarization was measured by varying the angle of the analyzer for a fixed polarizer angle of $30°$.

4 Results and Data Analysis

To begin, stability of a Neon-Helium (NeHe) gas laser and Neodynium Green laser was determined. First, the photodiodes signal was measured without any incident light in a dark room to determine the intensity of the background radiation and noise caused by the photodiode and amplifier. The measured value of the background radiation was:

$$U_{background} = (0.004 \pm 0.001) \quad [V]$$

After that, the photodiode was illuminated by the NeHe and green lasers for a period of $\sim$15 minutes. The graphs below denote the signal detected by the photodiode against time.

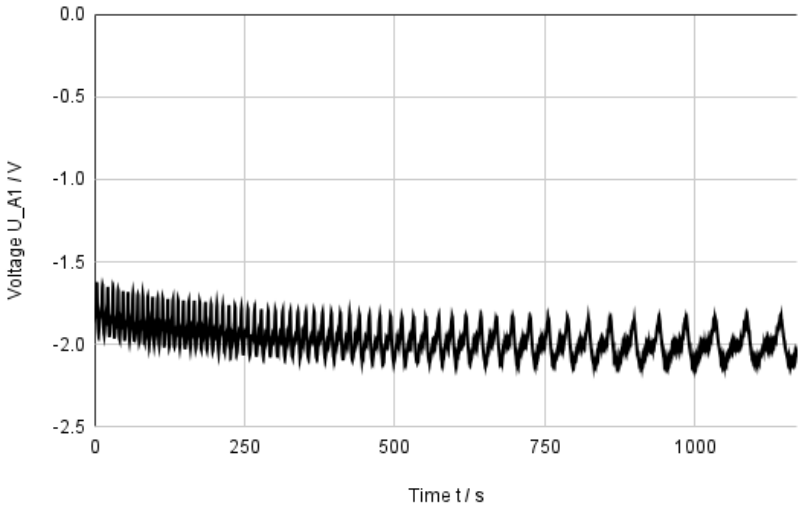

Figure 6: Plot of photodiode signal (V) against time (s) for NeHe laser

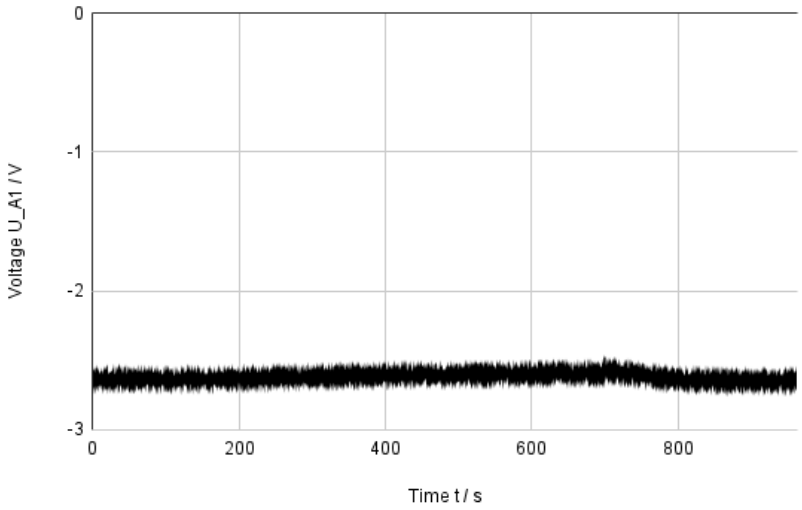

Figure 7: Plot of photodiode signal (V) against time (s) for Green laser

As one can observe, the stability of the two lasers varies a considerable amount. The NeHe laser exhibits periodic behavior which can be explained by the methods in which each laser beam is produced. The NeHe (Helium Neon) laser, produces light via ionization of Helium Neon gas. On the contrary, the light produced by the green laser is created by solid state crystals such as Neodynium alongside KTP (Potassium Titanyl Phosphate) doped crystals to produce green light (Paschotta, 2024). This method of light production makes the green laser more stable than the NeHe laser with intensity fluctuations. With the data collected, it is valid to conclude that the green laser is much more stable than the NeHe laser, and should therefor be used for the remaining duration of the experiment.

Now, let us determine the angle of polarization of the green laser in the fixture by

moving to setup 2, where a polarizer–which acts as an analyzer–is placed between the laser and the photodiode. By varying the angle of the analyzer, the intensity of the light should change accordingly and be measured by the photodiode. By consequently extracting the angle at which a maximum intensity is observed, one can trivially determine the angle of polarization of the green laser. Below denotes the table and plot of the raw data collected for the normalized photodiode signal against the rotation angle of the analyzer. Note that the error bars of the plot are too small to be qualitatively observed on the plot.

Table 1: Raw Data Table of Normalized Photodiode Signal I_A against Angle of Analyzer ϕ

Angle of Analyzer ($\pm 0.5°$)	Raw Photodiode Signal ($\pm 0.001V$)	Normalized Photodiode Signal ($\pm 0.002V$)
-90	0.276	0.170
-80	0.338	0.208
-70	0.471	0.290
-60	0.603	0.372
-50	0.828	0.510
-40	1.048	0.646
-30	1.238	0.763
-20	1.430	0.881
-10	1.564	0.964
0	1.623	1.000
10	1.577	0.972
20	1.432	0.882
30	1.232	0.759
40	0.998	0.615
50	0.765	0.471
60	0.519	0.320
70	0.361	0.222
80	0.277	0.171
90	0.255	0.157

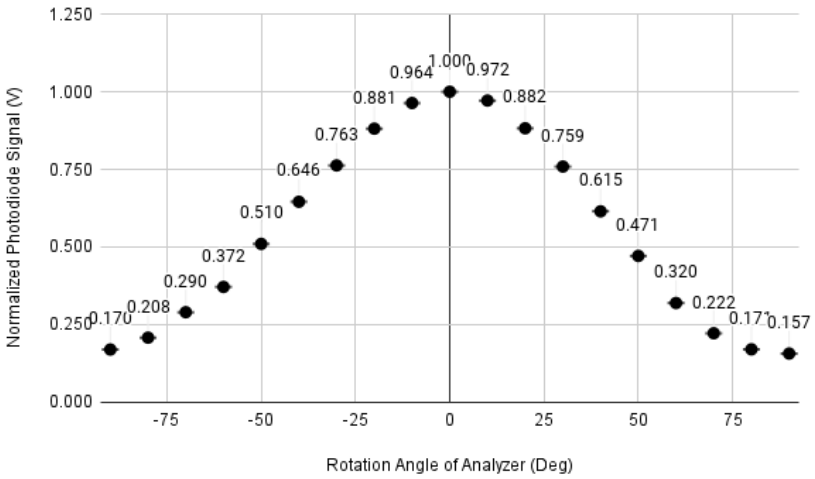

Figure 8: Plot of Normalized Photodiode signal (V) against orientation angle φ of analyzer

The graph above demonstrates the normalized intensity with respect to the angle of the analyzer φ. Since the maximum intensity occurs when the polarization direction of the green light aligns with the analyzer's orientation angle, we can conclude that the polarization direction of the green light was $0°$. After that the normalized signal voltage was plotted against the square of the cosine of the angle $\cos^2 \varphi$, where φ represents orientation angle of the analyzer. By Malus' law (equation 27) one expects a positive straight line trend to be reflected in the data with a slope equal to the incident intensity. Below is the table and plot of the results.

Table 2: Calculated data for Normalized Photodiode Signal against $\cos^2 \phi$ (Malus' Law)		
Normalized Photodiode Signal$(\pm 0.002V)$	$\cos^2 \phi$ (Angle between Polarization of Laser and Analyzer)	Error of $\cos^2 \phi$
0.170	0.00	0.0050
0.208	0.03	0.0014
0.290	0.12	0.0070
0.372	0.25	0.0087
0.510	0.41	0.0055
0.646	0.59	0.0007
0.763	0.75	0.0065
0.881	0.88	0.0087
0.964	0.97	0.0060
1.000	1.00	0.0000
0.972	0.97	0.0060
0.882	0.88	0.0087
0.759	0.75	0.0065
0.615	0.59	0.0007
0.471	0.41	0.0055
0.320	0.25	0.0087
0.222	0.12	0.0070
0.171	0.03	0.0014
0.157	0.00	0.0050

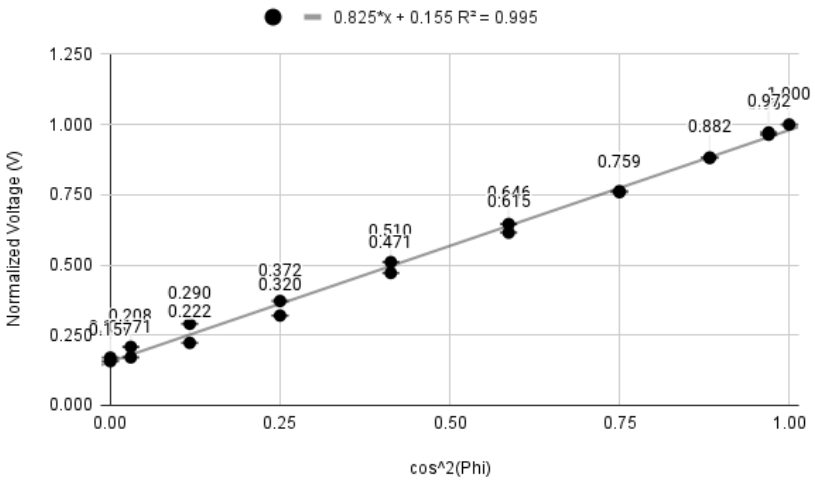

Figure 9: Plot of Normalized Photodiode signal (V) against orientation angle of analyzer

As one can observe from the graph, a strong linear correlation is present in our data, suggesting an agreement with Malus' law. The measured slope of the graph for the experimental values is:

$$I_{0,Experimental} = (0.825 \pm 0.155)[Wm^{-2}]$$

As the slope theoretically reflects the intensity of the light incident on the photodiode I_0, one should compare it to the theoretical value. It is important to note that the intensity is a different measurement than what is being taken by the photodiode (Amplified Voltage). Consequently, an alternative method must be employed to theoretically determine the slope based on theoretical assumptions. Now one calculates the intensity based the measurement of the angle and intensity of the maximum amplitude. To account for any shifts caused by background radiation, it is important to consider the minimum voltage at 0°, rather than state the theoretical minimum voltage to be 0. So, the theoretical value for the incident intensity on the photodiode is:

$$I_{0,Theoretical} = \frac{1 - 0.157}{\cos(0)^2 - \cos(90)^2} = 0.843 \pm 0.0014[Wm^{-2}]$$

Both values fall within eachothers' uncertainty, and agree with one another to a commensurable degree. In the next setup, the Brewster angle was studied qualitatively through the use of a polarizing filter in an informal setting. Observations specifically on water puddles were made, where it was noticed that by holding the polarizing lens at specific angles with respect to the planar surface of the puddle, the reflected light would fade. Reflecting on these results with the relevant theory, it is clear that as unpolarized light hits the surface of a different medium, it becomes polarized with a polarization axis parallel to the planar surface on which it is incident. It is clear that the minimum in observed intensity occurred at the Brewster angle, as all light

reflected by the puddle at the Brewster angle emerges polarized, and is therefore blocked by a perpendicularly rotated polarizer.

After this qualitative investigation and pursuit of intuition, the theoretical value of Brewster angle for the glass was calculated in preparation for the next aspect of the investigation. Applying formula 25, and using the theoretical value of the refractive index of glass given to us in the manual ($n_{glass} = 1.63$) one achieves:

$$\alpha = \arctan(n_{glass}) = \arctan(1.63) = 58.47^{\circ}$$

Fresnel's s- and p- reflection coefficients for the glancing case of incidence, when $\alpha = 90$ were determined to be -1 and 0 respectively by substituting the angle into formulas 21 and 22 respectively. Additionally, the formulas found for the reflection coefficients for the case of normal incidence were calculated as:

$$r^{\perp} = \frac{(n_{glass} - 1)^2}{n_{glass}^2 - 1} \qquad \text{(for normal incidence)}$$

$$r^{\parallel} = \frac{n_{glass} - 1}{n_{glass} + 1} \qquad \text{(for normal incidence)}$$

As it was required to rotate the green laser by 45 degrees, the maximum intensity at 0 degrees was measured to be $(1.765 \pm 0.004)V$, and the polarizer was then rotated by 45 degrees. The green laser was rotated again until the same maximum intensity was achieved. At 45 degrees, the highest achievable intensity was $(1.747 \pm 0.004)V$. After the adjustment of the laser orientation, the photodiode signal of primary and reflected intensities of light using s- and p- polarization was measured. The angle was varied from 15° to 85° in steps of 5°. Below denote the tables of raw data containing the values of the photodiode signal against the prism rotation angle for p- and s- polarization respectively. The following data is then used to calculate the Fresnel Reflection Coefficients.:

Table 3: Photodiode Signal (V) against Rotation Angle (Degrees) for P-Polarization		
Rotation Angle (Deg)	Photodiode Signal (V) (+- 0.001 V)	Normalized Photodiode Signal (v)
15	0.34	0.119
20	0.308	0.108
25	0.27	0.094
30	0.183	0.062
35	0.165	0.055
40	0.122	0.039
45	0.085	0.026
50	0.039	0.009
55	0.003	0.004
60	0.014	0.000
65	0.069	0.020
70	0.22	0.075
75	0.776	0.280
80	1.783	0.650
85	2.721	0.994

Table 4: Photodiode Signal (V) against Rotation Angle (Degrees) for S-Polarization		
Rotation Angle (Deg)	Photodiode Signal (V) (+-0.001V)	Normalized Photodiode Signal (v)
15	0.278	0.072
20	0.283	0.0730
25	0.308	0.080
30	0.345	0.090
35	0.368	0.096
40	0.438	0.115
45	0.478	0.126
50	0.591	0.157
55	0.784	0.209
60	0.973	0.261
65	1.229	0.331
70	1.643	0.443
75	2.218	0.599
80	2.874	0.779
85	3.672	0.996

After collecting the data for the observed reflected intensity with respect to the incident angle on the prism, it was necessary to apply these values to formula 24. To do so, the primary intensities for both p- and s- polarization were taken (based on the orientation of the polarizer). These values were measured as:

$$\text{Primary intensity for s-polarization: } 0.264 \pm 0.001[V]$$

$$\text{Primary intensity for p-polarization: } 0.273 \pm 0.001[V]$$

Using these values, the calculated data for the Fresnel coefficients at each angle was found by substituting the tables' values into formula 24. Below is the data of the calculated data points based on the raw data. After this the data was normalized with respect to the maximum Fresnel coefficient to be consistent with the values obtained via a theoretical calculation.

Table 5: Fresnel Reflection Coefficient against Angle of Reflection for S-Polarization from measured values		
Incident Angle ($\pm 0.5°$)	Calculated Fresnel Reflection Coefficient	Normalized Fresnel Reflection Coefficient
15	0.521	0.268
20	0.526	0.271
25	0.550	0.283
30	0.583	0.300
35	0.603	0.311
40	0.661	0.340
45	0.691	0.356
50	0.771	0.397
55	0.891	0.459
60	0.994	0.512
65	1.119	0.576
70	1.296	0.667
75	1.507	0.776
80	1.717	0.884
85	1.942	1.000

Table 6: Fresnel Reflection Coefficients against Angle of Reflection for P-Polarization from measured values		
Incident Angle ($\pm 0.5°$)	Calculated Fresnel Reflection Coefficient	Normalized Fresnel Coefficients
15	0.661	0.347
20	0.628	0.329
25	0.586	0.307
30	0.476	0.249
35	0.449	0.235
40	0.380	0.199
45	0.307	0.161
50	0.180	0.094
55	0.127	0.067
60	0.037	0.019
65	0.270	0.141
70	0.525	0.275
75	1.012	0.530
80	1.543	0.808
85	1.909	1.000

To ensure the accuracy of the calculated data displayed in the tables above, it is important to compare them to theoretical values. To find the theoretical values for the Fresnel Coefficients, formulas 21 and 22 were applied to angles from 15 degrees to 85 degrees with a theoretical refractive index of 1.63. Below are the tables generated by the angles 15 to 85 using this method.

Table 7: Theoretical Fresnel Coefficients based on Derived Formula for s-polarization for theoretical angles	
Incident Angle ($\pm 0.5°$)	Calculated Fresnel Reflection Coefficient
15	0.250
20	0.258
25	0.269
30	0.284
35	0.301
40	0.323
45	0.350
50	0.382
55	0.421
60	0.468
65	0.524
70	0.591
75	0.671
80	0.764
85	0.873

Table 8: Theoretical Fresnel Coefficients based on Derived Formula for p-polarization for theoretical angles	
Incident Angle ($\pm 0.5°$)	Calculated Fresnel Coefficient
15	0.229
20	0.221
25	0.209
30	0.195
35	0.176
40	0.152
45	0.123
50	0.086
55	0.039
60	0.019
65	0.094
70	0.189
75	0.313
80	0.476
85	0.696

Now with both the measured and calculated theoretical values of the Fresnel Coefficients, one can compare the two plots graphically to analyze the accuracy of the measurements taken during the investigation. Both data sets are placed on the same graph below to allow visual comparison.

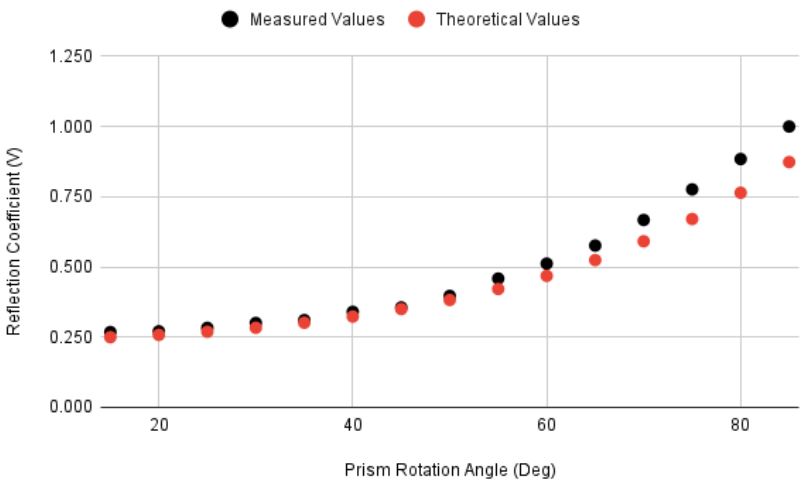

Figure 10: Plot of photodiode signal (V) against incidence angle of the light in the prism (s-polarization)

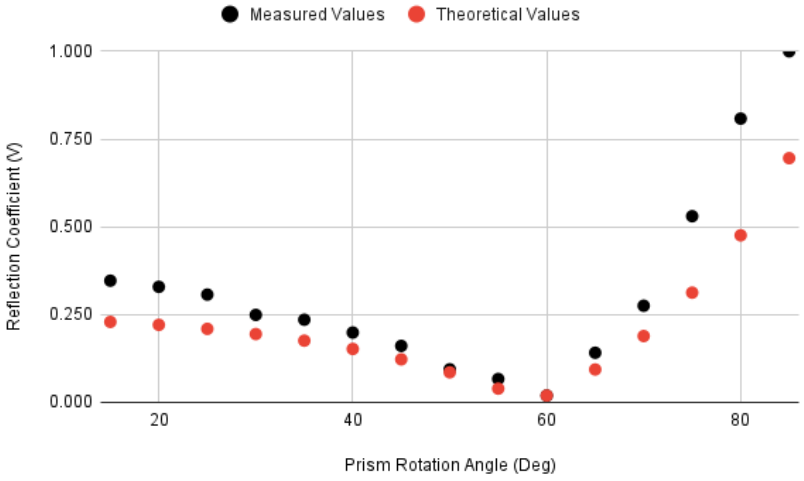

Figure 11: Plot of photodiode signal (V) against incidence angle of the light in the prism (p-polarization)

Observing the graphs above, it is clear thart our data is correlated appropriately to the theoretical values. However, some slight deviations are observed on the ends of either graph. Despite these deviations, a clear trend is observed. Using the angle which yields the minimum intensity of the p-polarization plot, the Brewster angle can be calculated. From the graph above, it is clear that the Brewster angle is approximately 60 degrees. Using this measurement, one can substitute the value into equation 25 to find the refractive index. Doing so, the calculated refractive index based on the limited measurements is:

$$n_{glass} = \tan(\alpha_B) = \tan 60^\circ = 1.732 \pm 0.0087$$

To measure the rotation of the polarization vector in this setup, the photodiode was illuminated by the reflected beam and the angle of the analyzer filter was varied until maximum value of the signal was found in both rotational direction. However, due to the low precision of the equipment and the small values that were required to make a meaningful conclusion from the data, this extra investigation step was deemed impossible. See the results below:

Angle of incidence ± 0.5 (Deg)	Clockwise rotational angle of analyzer ± 0.5 (Deg)	Counterclockwise rotational angle of analyzer ± 0.5 (Deg)	Averaged Polarization Angle ± 0.5 (Deg)
15	4	6	5
20	3	4	3.5
25	5	6	5.5
30	4	5	4.5
35	5	6	5.5
40	2	3	2.5
45	6	6	6
50	4	5	4.5
55	5	3	4
60	4	6	5
65	5	5	5
70	4	5	4.5
75	6	5	5.5
80	2	2	2
85	4	3	3.5

It was noticed that due to the high precision required of the measurements, it was impossible to distinguish the proper angle required to observe a sufficient difference in the changed angle. Due to the noise caused by the amplification of the signal, it was additionally impossible to measure given the amplifier used. Manual observation was also attempted for the maxima by rotating the polarizing lens, but this method again was not very fruitful as the data appeared the same for each angle.

The next part of the investigation focused on analyzing the behavior of quarterwave and halfwave plates and their polarization properties. To begin, it was crucial to ensure that the stability of the lamp was nominal for the investigation. To do so, the signal from the lamp incident on the photodiode was measured with a polarizing angle of 0 degrees for 10 minutes. For the first 15 seconds, the light was switched off as a means of concomitantly determining the background radiation of the photodiode in the dark to be used as an offset value in later measurements. It is qualitatively clear from the graph below that the lamp is sufficiently stable for meaningful measurements to be made.

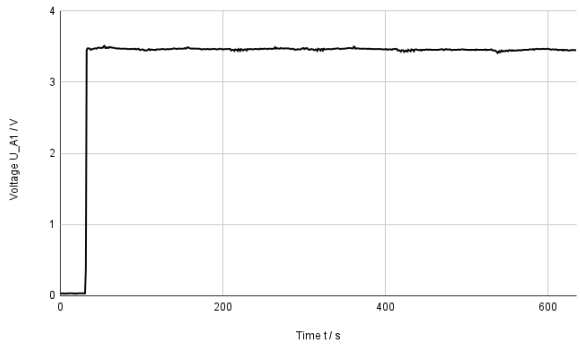

Figure 12: Voltage Signal (V) of Photodiode against Time Elapsed (s)

Moving on, the quarterwave plate was positioned such that its ordinary axis was aligned to the optic axis of the 0 degree angle polarizer. After the light passes through the first polarizer and then through the quarterwave plate, the light passes through an analyzer which is rotated through an angle of $-90°$ to $90°$. The intensity of the light is measured through all rotations of the analyzer for angles of the polarizer $0°, 30°, 45°, 60°, 90°$. As there is a very large amount of data associated with these measurements, only the graphs will be displayed. Below the graph of the measured photodiode intensities against analyzer angle is plotted for each rotation of the initial polarizer.

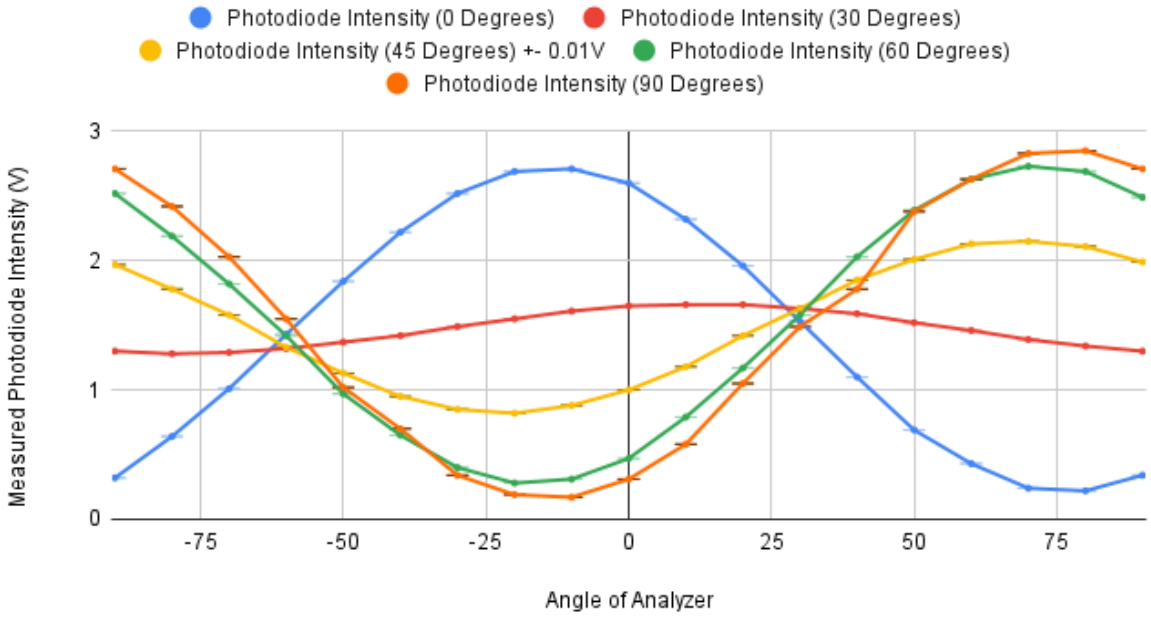

Figure 13: Graph of Measured Photodiode Intensity (V) against Angle of Analyzer (Degrees) for Fixed Polarizer Angles

The data displayed in the plot above demonstrates the behavior of the intensity of the linearly polarized light incident on the photodiode after being circularly polarized by the quarterwave plate. The transition between the Ordinary optic (OR) axis and Extraordinary (EO) optic axis is clear by the variation in the maximum intensity for each polarization pattern. For the photodiode intensity for a corresponding polarizer angle of 0 degrees, the maximum intensity is large in comparison to the intensities observed in the polarization patterns for polarizer angles of 30 and 45 degrees. Furthermore, the maximum intensity of the polarization patterns with angles closer to 90 degrees are much larger, implicitly implying polarization via the Extraordinary (EO) polarization axis. Qualitatively, and quantitatively, the data gathered for this part of the experiment accurately reflect the expected behavior of the intensity for the given quarterwave plate configuration.

Now, similar measurements are taken, however, instead of varying the angle of the

polarizer, the polarizer will be fixed at an angle of 0 degrees, and the quarterwave plate will be varied at fixed angles $0°, 30°, 45°, 60°$ and $90°$ respectively. Below is the plot of the results tied to using this method.

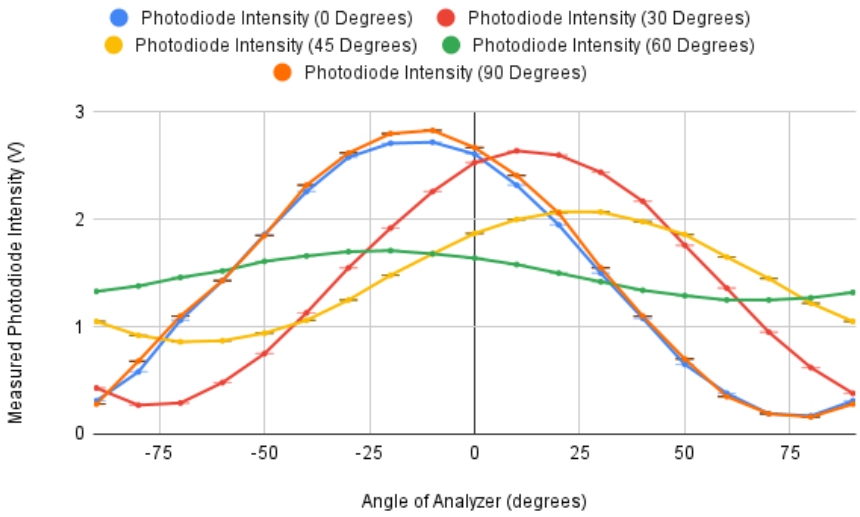

Figure 14: Plot of measured Photodiode intensity (V) against Analyzer Angle (Degrees) for varying Quarterwave Plate Angle

This graph again beautifully demonstrates the two optical axes of the birefringent crystal in a clear manner. Note how the Photodiode Intensity polarization patters for quarterwave plate orientations $0°$ and $90°$ are almost exactly the same. As the quarterwave plate rotates from 0 to 90 degrees, the light is first polarized by the Ordinary axis, and then the Extraordinary axis, which lies orthogonal to the latter. This is exactly why we see a complete match in the curves corresponding to each of these angles. Additionally, one can observe that

5 Error Analysis

For all errors involving the slope of the graph, the uncertainty of the slope was approx- imated using the built-in function (LINEST), which works by approximating the linear slope of a set of data points through the least squares method. As a byproduct, the error of the slope is given in absolute form. Due to the efficiency of this method, and the large quantity of graphs, it was the clear choice for this investigation.

For all errors involving the slope of the graph, the uncertainty of the slope was approx- imated using the built-in function (LINEST), which works by approximating the linear slope of a set of data points through the least squares method. As a byproduct, the error of the slope is given in absolute form. Due to the efficiency of this method, and the large quantity of graphs, it was the clear choice for this investigation.

For all errors involving numerical calculations with propagated error, such as for the uncertainties of the final measurements, the root sum of squares method (RSS) was employed. This method involves calculating the propagated error of a formulaic value by computing all partial derivatives with respect to all error prone parameters, and taking it under a square root. The formula for this is given below.

$$\Delta y = \sqrt{\sum_{i=0}^{n} \left(\frac{\partial y}{\partial x_i} \cdot \Delta x_i \right)^2} = \sqrt{\left(\frac{\partial y}{\partial x_1} \cdot \Delta x_1 \right)^2 + \cdots + \left(\frac{\partial y}{\partial x_n} \cdot \Delta x_n \right)^2} \tag{30}$$

One of the possible systematic error in this experiment could be possibly caused by background radiation. The background radiation was substracted from all measurements to account error of the noise when measuring photodiode signal. The uncertainty in this measurement can cause systematic error across all photodiode signal recordings. Possible errors can also be caused by the NeHe and green lasers. But as their stability were determined, the green laser was chosen, as it showed more stable behavior. In this way, errors caused by the stability of the laser were reduced to a minimum.

When determining the angle of polarization, the table and plot of the normalized photodiode signal against the rotation angle of the analyzer showed minimal error bars. The angle measurements had an uncertainty of $\pm 0.5^\circ$. Since the normalized signal error is raw signal data at some angle divided by raw signal data at 0°, to determine the error of the normalized signal, a fractional error formula was used. In this case the errors were too minimal relative to the data measurements.

For Verification of Malus' Law, error of the experimental slope was calculated using "LINEST" function. For the theoretical value of the $I_{0,Theoretical}$, again, RMS method was used:

$$\Delta I = \sqrt{2 \left(\frac{\Delta V_1}{\cos^2(\alpha_1) - \cos^2(\alpha_2} \right)^2 + \left(\frac{(V_1 - V_2) \sin 2\alpha_1}{\left(\cos^2 \alpha_1 - \cos^2 \alpha_2\right)^2} \cdot \Delta \alpha_1 \right)^2 + \left(\frac{(V_1 - V_2) \sin(2\alpha_2)}{\cos^2 \alpha_1 - \cos^2 \alpha_2)^2} \cdot \Delta \alpha_2 \right)^2} \tag{31}$$

Experimental slope had bigger uncertainty compared to the theoretical one, which can suggest significant measurement errors, which can be caused by alignment issues, laser fluctuations or angle inaccuracies.

6 Discussion

7 Conclusion

References

Paschotta, R. (2024, Oct). *Green lasers.* RP Photonics Encyclopedia. RP Photonics AG. Retrieved 2024-10-06, from https://www.rp-photonics.com/green_lasers.html (Available online at https://www.rp-photonics.com/green_lasers.html) doi: 10.61835/lcy

Wagner, V., & Söcker, T. J. (2024). Advanced physics lab 1 manual. *Constructor University*.